Atmospheric Research 336 (2026) 108915

Contents lists available at ScienceDirect

Atmospheric Research

journal homepage: www.elsevier.com/locate/atmosres

# Distinct mechanisms and sub-seasonal prediction of daytime, nighttime, and compound heatwaves in southern China: The role of intra-seasonal oscillations

Kaiqi Wang [a,b], Tuantuan Zhang [a,b,*], Song Yang [a,b], Fei Liu [a,b], Weiwei Wang [c,d], Wenshi Lin [a,b], Lianlian Xu [a,b,*], Yanheng Luo [a,b], Haiyang Xue [a,b]

[a] School of Atmospheric Sciences, Sun Yat-sen University, and Southern Marine Science and Engineering Guangdong Laboratory (Zhuhai), Zhuhai 519082, China
[b] Guangdong Province Key Laboratory for Climate Change and Natural Disaster Studies, Sun Yat-sen University, Zhuhai 519082, China
[c] Meteorological Bureau of Shenzhen Municipality, Shenzhen 518040, China
[d] Shenzhen Key Laboratory of Severe Weather in South China, Shenzhen 518040, China

ARTICLE INFO

*Keywords:*
Heatwaves
Intra-seasonal oscillations
Sub-seasonal prediction
Southern China

ABSTRACT

Different heatwave types are linked to distinct physical processes; however, the influence of intra-seasonal oscillation (ISO) patterns on the variability and sub-seasonal prediction of daytime, nighttime, and compound heatwaves remains insufficiently understood. In this study, the underlying mechanisms for the three types of heatwaves over southern China (SC) during 1999–2022 and the major sources of their sub-seasonal prediction skill are identified. The results show that daytime heatwaves over SC are largely driven by extra-tropical ISO-induced anticyclonic circulation, creating hot and dry conditions. Nighttime heatwaves are primarily modulated by tropical ISO, which induces an anomalous anticyclone to the southeast of SC. The associated southerly flow transports excess moisture into the region, creating cloudy and moist conditions that facilitate nighttime heatwaves. Evaluation of outputs from the NCEP Climate Forecast System Version 2 and the European Centre for Medium-Range Weather Forecasts demonstrates that reliable forecasts for daytime and nighttime heatwaves rarely extend beyond a two-week horizon. In comparison, compound heatwaves exhibit more intense surface temperature and closer linkages with both tropical and extra-tropical ISOs, thereby maintaining superior sub-seasonal prediction skills than the other two heatwave types. Our study highlights that the enhanced influence of intra-seasonal oscillations, especially those of tropical origin, offering a promising avenue for sub-seasonal predictions of regional heatwaves.

## 1. Introduction

The frequency, intensity, and duration of heatwaves increase rapidly across widespread regions under global warming, exerting severe stress on agricultural production, socio-economic systems, and human health (Robinson, 2001; Meehl and Tebaldi, 2004; Robine et al., 2008; Gasparrini and Armstrong, 2011; Perkins and Alexander, 2013; Sun et al., 2014; You et al., 2017). According to statistics, the heatwave-attributable mortality consistently ranks one of the highest among climate extremes during the recent decades (Bell et al., 2018). Climate projections have indicated that the frequency and severity of heatwaves would continue to rise steadily (Chen and Li, 2017; Li et al., 2017; Wang et al., 2020). Understanding the underlying mechanisms and improving the prediction of heatwave occurrence are essential for disaster preparation and climate adaptation.

Distinct mechanisms underlying different types of heatwaves—daytime, nighttime, and compound heatwaves—have been substantially identified by previous studies (Chen and Lu, 2014; Lu and Chen, 2016; Luo et al., 2022; Luo et al., 2025; Wu et al., 2023). Typically, daytime heatwaves are driven by persistent anticyclonic circulations that induce dry and clear-sky conditions, thereby enhancing surface absorption of incoming shortwave radiation and leading to a rising daytime temperature (Della-Marta et al., 2007; Dole et al., 2011; Schubert et al., 2011; Trenberth and Fasullo, 2012; Lau and Kim, 2012;

* Corresponding authors at: School of Atmospheric Sciences, Sun Yat-sen University, and Southern Marine Science and Engineering Guangdong Laboratory (Zhuhai), Zhuhai 519082, Guangdong, China.
*E-mail addresses:* zhangtt75@mail.sysu.edu.cn (T. Zhang), xullian@mail.sysu.edu.cn (L. Xu).

https://doi.org/10.1016/j.atmosres.2026.108915
Received 28 November 2025; Received in revised form 26 February 2026; Accepted 8 March 2026
Available online 9 March 2026

Gao et al., 2018b). The drivers of such high-pressure systems triggering heatwaves are complex and vary by regions (Loikith and Broccoli, 2012; Ding et al., 2010; Luo and Lau, 2017; Pfahl et al., 2015; Qian et al., 2024). For nighttime heatwaves, they are generally characterized by humid and cloudy conditions, which enhance downward longwave radiation and prolong elevated temperatures throughout the night (Meehl and Tebaldi, 2004; Li et al., 2017; Thomas et al., 2020). Chen and Lu (2014) indicated that the occurrence of hot nights in Beijing was primarily attributed to northward moisture transport over eastern China. Compound heatwaves, which are herein defined as the concurrent occurrence of daytime and nighttime heatwaves, combine the characteristics of both types. They are typically driven by high-pressure systems that lead to less cloud cover, and are coupled with increased water vapor transport (Hong et al., 2018; Li et al., 2020; Li et al., 2021; Luo et al., 2025). Despite the elucidation of the mechanisms responsible for the three types of heatwaves, a systematic comparison of their respective prediction skill and sources remains lacking.

Sub-seasonal prediction serves to bridge the gap between weather forecasts and climate predictions, offering important opportunities for improved risk management (Vitart et al., 2017; Vitart and Robertson, 2018). Several studies have demonstrated that the low-frequency oscillations, including the Boreal Summer Intra-seasonal Oscillation (BSISO)/the Madden-Julian Oscillation (MJO) and the 10–30-day quasi-biweekly oscillation (QBWO), are important sources of sub-seasonal heatwave predictability (Pegion and Sardeshmukh, 2011; Waliser et al., 2003; Xie et al., 2020; Yang et al., 2018; Wang et al., 2025). For instances, the sub-seasonal prediction skill of heatwave intensity and duration over the Yangtze River Basin highly depends on the model's performance in capturing intra-seasonal variability (Qi and Yang, 2019; Xie et al., 2020). Hsu et al. (2020) suggested that the sub-seasonal prediction of heatwaves over northeastern China is significantly influenced by the model capability in simulating the MJO. Models that better reproduce the intensity of the MJO in the western Pacific warm pool region tend to exhibit higher forecast skill at a lead time of 1–4 weeks (Hsu et al., 2020). However, how intra-seasonal oscillations and their phase-dependent atmospheric anomalies differentially influence various heatwave types and their predictions are not yet well understood.

Southern China, a hotspot for intense and frequent heatwaves, has become increasingly vulnerable due to its high climatological temperatures and dense urbanization (Chen and Li, 2017; Gao et al., 2018a, 2018b; You et al., 2017). Intra-seasonal oscillations such as the MJO/BSISO and QBWO play essential roles in modulating the weather and climate variability, including regional heatwaves, over this region (Krishnamurti and Ardanuy, 1980; Annamalai and Slingo, 2001; Jia and Yang, 2013; Matsueda and Takaya, 2015; Diao et al., 2018; Dong et al., 2020; Gao et al., 2020; Wang et al., 2025). Previous studies have indicated that different intra-seasonal oscillations and their varying phases exert distinct influences at different stages of southern China heatwaves (Chen et al., 2016, 2018; Zheng et al., 2022; Huang et al., 2025; Wang et al., 2025). Recently, Li et al. (2024) revealed the combined influence of 10–30-day tropical and mid–high latitude intraseasonal oscillations on the rapid increases of humid heatwaves in southern China. These systems drive changes in atmospheric circulations that modulate regional adiabatic heating and moisture flux transport (Jiang et al., 2004; Mao and Chan, 2005; Lee et al., 2013; Oh and Ha, 2015; Fang et al., 2017; Wang et al., 2018), which may play distinct and yet unexplored roles in modulating different types of heatwaves over southern China.

Based on these premises, this study aims to investigate the distinct physical mechanisms and sub-seasonal prediction of daytime, nighttime, and compound heatwaves over southern China, with a focus on the specific role of tropical and extra-tropical intraseasonal oscillations. The rest of the paper is organized as follows. Datasets and methods are described in Section 2. Section 3 presents the distinct features associated with three types of heatwaves. Section 4 depicts the role of intra-seasonal oscillations. Section 5 describes the influence of intra-seasonal oscillations on the sub-seasonal prediction of different heatwave types. A summary of the main findings along with further discussion are provided in Section 6.

## 2. Data and methods

### 2.1. Data

The daily maximum (Tmax) and minimum (Tmin) 2-m temperatures are obtained from the CN05.1 dataset with a horizontal resolution of $0.25^\circ \times 0.25^\circ$, which is constructed using daily observations from more than 2400 meteorological stations in China, covering the period of 1961–2022 (Wu and Gao, 2013). Daytime, nighttime, and compound heatwave events are selected based on the CN05.1 in this study. The CN05.1 has been extensively validated and widely applied in climate change detection, extreme event analysis, and model performance evaluation (Wang et al., 2018; Zhou et al., 2014). In this study, we focus on the summer season (May–September, MJJAS) for heatwave-related assessments and model evaluations. To investigate physical processes associated with different heatwave types, we analyze daily atmospheric variables derived from the European Centre for Medium-range Weather Forecasts Reanalysis v5 (ERA5) at a horizontal resolution of $1^\circ \times 1^\circ$ (Hersbach et al., 2020). These variables include outgoing longwave radiation (OLR), relative humidity, precipitation, surface latent heat flux, surface sensible heat flux, 500-hPa geopotential height, and 500-hPa and 850-hPa winds. The daily anomalies of variables are obtained by subtracting their respective climatologies for the corresponding day.

Outputs from the NCEP Climate Forecast System Version 2 (CFSv2) and the European Centre for Medium-Range Weather Forecasts Subseasonal-to-Seasonal (ECMWF S2S) prediction system are used for sub-seasonal prediction analysis (Saha et al., 2014; Vitart, 2014). The ECMWF system is initialized twice a week (on Mondays and Thursdays) at 0000, 0600, 1200, and 1800 UTC, whereas the reforecasts of NCEP CFSv2 are initialized at 0000, 0600, 1200, and 1800 UTC per day. Forecast verification is conducted using the ensemble mean of the four initializations on a given day for each S2S model. To more conveniently compare the prediction skills between the two models, we adopted a data processing method proposed by previous studies (Yang et al., 2018; Qi and Yang, 2019) to reprocess the twice-weekly data of the ECMWF model outputs to daily reforecast data (as in the NCEP models). Briefly, for a given lead time of N days, ECMWF forecasts from $N-2$ to $N+2$ days are used to represent the N-day lead prediction. When two forecasts are available for the same lead time, an arithmetic mean is applied. Previous sensitivity tests have demonstrated that this reconstruction procedure does not alter the main conclusions derived from either the reconstructed daily reforecast data or the original twice-weekly outputs (Yang et al., 2018). We analyze daily outputs of Tmax, Tmin, zonal winds, and 500-hPa geopotential height from the 45-day reforecasts produced by the CFSv2 and ECMWF during the period 1999–2022. The lead time for a target day is up to 44 days. The 0-day (44-day) lead denotes that the model runs are initialized on the current day (44 days ago). For convenience, LD0, LD1, LD2, …, and LD44 represent the outputs of 0-day lead, 1-day lead, 2-day lead, …, and 44-day lead, respectively.

### 2.2. Definitions of heatwaves and BSISO

Currently, there is a lack of universally standardized definition of heatwaves across climate and public health disciplines (Robinson, 2001; Wang et al., 2017; You et al., 2017). In this study, different types of heatwaves are identified using percentile-based thresholds with duration constraints, similar to those adopted in previous studies (Luo et al., 2022; Luo et al., 2025). Specifically, compound heatwaves are identified if both daily Tmax and Tmin exceed their corresponding calendar 90th percentile values (derived from all summer days during 1999–2022) for at least three consecutive days. A daytime heatwave is defined as a

period of at least three consecutive days where daily Tmax exceeds its 90th percentile, while the daily Tmin does not. A nighttime heatwave is defined analogously, with the roles of Tmax and Tmin reversed. Here, the relative threshold is defined as the 90th percentile of daily Tmax and Tmin, calculated from all summer days during the reference period of 1999–2022. Heatwaves in observations and models are selected based on their respective observed and lead-time-dependent thresholds.

The boreal summer intraseasonal oscillation (BSISO) indices are constructed using a multivariate empirical orthogonal function (MV-EOF) of OLR and 500-hPa zonal wind (U500) anomalies analysis over the Asian summer monsoon domain (10°S–40°N, 40°E–160°E) (Jiang et al., 2004; Lee et al., 2013). Daily anomalies of OLR and U500 are obtained by removing the climatology over the 1999–2022. To extract intraseasonal variability, the anomaly fields are further band-pass filtered using a Butterworth filter (Selesnick and Burrus, 2002) for two frequency bands: 10–30-day and 30–60-day. The first two leading modes (PC1 and PC2) of the MV-EOF present the BSISO1-related signals with a period of approximately 30–60-day, which propagate northwards/northeastwards from the tropical Indian Ocean towards East Asia. The third and fourth MV-EOF modes (PC3 and PC4) capture the northwestward propagating BSISO2 from the tropical central-western Pacific towards East Asia with a period of approximately 30–60-day. The life cycle of each BSISO component can be divided into eight distinct phases by constructing phase diagrams of the corresponding principal components (PCs). If a BSISO component has an amplitude less than 1, it is categorized as an insignificant BSISO signal. For model forecasts, BSISO indices are calculated from the initialized (raw) forecasts. Forecast anomalies at each lead time are obtained by removing a hindcast-based lead-time-dependent climatology. To ensure consistency with the observational BSISO definition, the predicted BSISO1 and BSISO2 states were obtained by projecting the modeled OLR and U500 anomalies at different forecast lead times onto the observed MV-EOF modes.

### 2.3. Methods

To diagnose the propagation of large-scale Rossby wave trains associated with different types of heatwaves over southern China, the horizontal Takaya-Nakamura wave activity flux (WAF) is applied, based on the ERA5 reanalysis dataset:

$$W=\frac{p\cos\varphi}{2|U|}\begin{Bmatrix}\frac{U}{a^2cos^2\varphi}\left[\left(\frac{\partial\psi'}{\partial\lambda}\right)^2-\psi'\frac{\partial^2\psi'}{\partial\lambda^2}\right]+\frac{V}{a^2\cos\varphi}\left[\frac{\partial\psi'}{\partial\lambda}\frac{\partial\psi'}{\partial\varphi}-\psi'\frac{\partial^2\psi'}{\partial\lambda\partial\varphi}\right]\\ \frac{U}{a^2\cos\varphi}\left[\frac{\partial\psi'}{\partial\lambda}\frac{\partial\psi'}{\partial\varphi}-\psi'\frac{\partial^2\psi'}{\partial\lambda\partial\varphi}\right]+\frac{V}{a^2}\left[\left(\frac{\partial\psi'}{\partial\varphi}\right)^2-\psi'\frac{\partial^2\psi'}{\partial\varphi^2}\right]\end{Bmatrix} \quad (1)$$

where the overbar and prime represent the climatological mean and anomaly. $\psi'$ denotes the perturbation streamfunction. The background flow (U, V) is defined as the daily climatological mean wind field at 500-hPa, calculated over the full study period. $|U|$ represents the horizonal wind speed, $\varphi$ is the latitude, $\lambda$ is the longitude, and $p$ is the pressure.

As shown in Eq. (2), the Heidke Skill Score (HSS; Heidke, 1926) quantifies forecast accuracy by estimating the proportion of correct predictions while adjusting for those that could occur by random chance (Hyvärinen, 2014). The HSS offers a clear evaluation of forecast skill relative to a reference value, and has been widely applied in previous studies on seasonal forecast verification (Barbero et al., 2017; Higgins et al., 2004; Kowal et al., 2023; Walker et al., 2019). Traditional skill scores such as the Threat Score and Equitable Threat Score are often sensitive to the base rate (i.e., the relative frequency of the event), and their values tend to decrease to zero as the event becomes more extreme. Because the frequency of extreme events varies significantly across regions due to local climate conditions, metrics like the Threat Score may not offer an objective assessment of forecast skill for extremes (Schaefer, 1990; Stephenson, 2000). To address this issue, Ferro and Stephenson (2011) proposed the Extremal Dependence Index (EDI), which remains robust regardless of event rarity and does not rely on the base rate. Therefore, this study employs both the HSS and the EDI metrics to evaluate sub-seasonal prediction skill of heatwaves. The HSS and EDI are defined as follows:

$$HSS=\frac{2(ad-bc)}{(a+c)(c+d)+(a+b)(b+d)} \quad (2)$$

$$EDI=\frac{\log F-\log H}{\log F+\log H} \quad (3)$$

$$F=b/(b+d)\ H=a/(a+c) \quad (4)$$

$a$, $b$, $c$, and $d$ stand for hit, false alarm, miss, and correct rejection, respectively. $F$ is the false alarm rate, and $H$ is the hit rate. HSS and EDI range from $-\infty$ to 1, $-1$ to 1 individually. A negative value indicates that the random forecast is better, while a value of zero means no skill. A perfect prediction obtains a value of 1.

To elucidate the basic physical mechanisms, composite analyses are performed for daytime, nighttime, and compound heatwaves. The seasonal cycle is removed by subtracting the climatological daily mean from each variable before constructing composites. All significance tests of the composite anomalies are conducted based on the Student's $t$-test. As these heatwave events are typically separated in time, and the influence of serial autocorrelation is largely mitigated, temporal autocorrelation is not considered when estimating degrees of freedom for composite results. To assess whether the forecast skill exceeds that expected by chance, statistical significance of HSS and EDI is evaluated using a bootstrap resampling approach.

## 3. Distinct features associated with three types of heatwaves

Fig. 1 shows frequencies and trends of daytime, nighttime, and compound heatwaves over southern China during MJJAS 1999–2022. Daytime heatwaves are primarily concentrated over the northern flank of southern China, with a regional-averaged frequency of 1.8 days per year (Fig. 1a). The occurrence of nighttime heatwaves is also limited during the recent two decades, with an area-averaged frequency of 2.4 days (Fig. 1b). The occurrence of compound heatwaves is the most frequent in comparison, with a regional-averaged frequency of about 4 days per year (Fig. 1c). While southern China is a hotspot for both the frequency and trend of compound heatwaves, the occurrence and trends of the other two heatwave types are notably less pronounced (Fig. 1). The occurrence dates of different heatwave types are presented in Fig. S1. Daytime heatwaves predominantly occur from August to September, whereas compound and nighttime heatwaves are concentrated from June to August (Fig. S1). Notably, the temporal window for compound heatwave occurrences appears to be broadening (Fig. S1). This highlights the growing threat of compound heatwaves in the region.

Previous studies have indicated that distinct local mechanisms underlie different types of heatwaves (Luo et al., 2022; Luo et al., 2025; Wu et al., 2023). Fig. 2 displays several regional-averaged key variables linked to daytime, nighttime, and compound heatwaves over southern China. During daytime heatwaves, decreases in total cloud cover and relative humidity enhances downward shortwave radiation and surface net radiation (Fig. 2b–d). The elevated surface temperature is also accompanied by an increase in latent and sensible heat fluxes (Fig. 2e–f). In contrast, positive cloud cover and relative humidity anomalies are observed over southern China during nighttime heatwave period (Fig. 2b–c). These conditions lead to a reduction in daily net radiation (Fig. 2d) but induce significant positive anomalies in downward longwave radiation at night, which mitigates surface heating during the daytime while sustains high temperatures at night (Chen and Lu, 2014; Luo et al., 2022; Luo et al., 2025; Wu et al., 2023). Correspondingly, nighttime heatwaves accompanied by negative anomalies of sensible

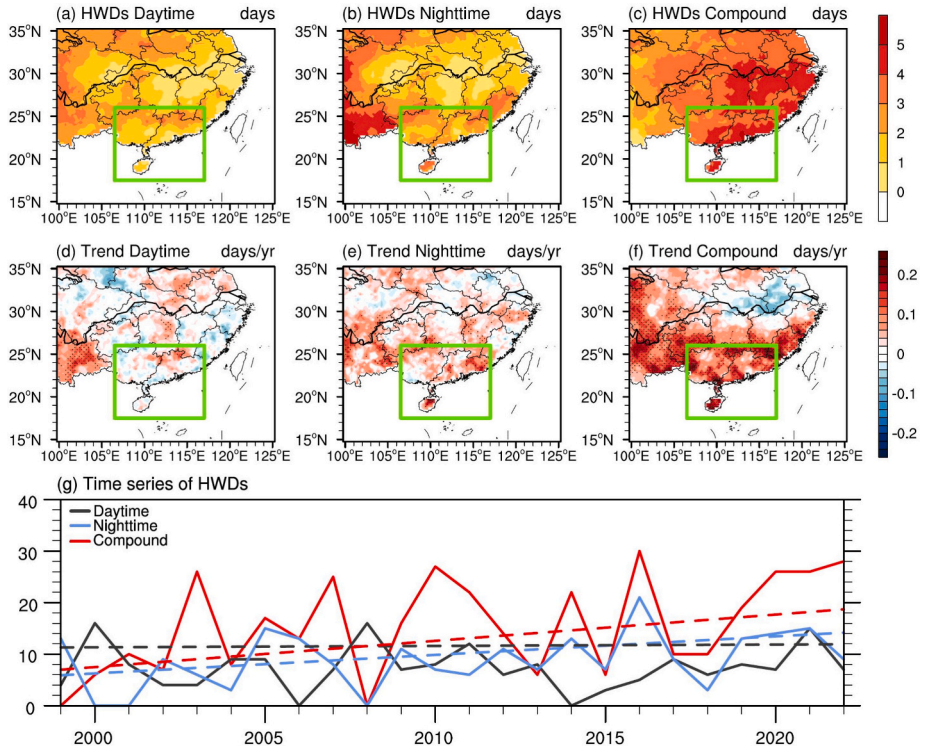


**Fig. 1.** (a–f) Climatological heatwave days (HWDs; days) and long-term trends (day $yr^{-1}$) of daytime, nighttime, and compound heatwaves in MJJAS over southern China during 1999–2022. (g) Time series of frequency of daytime (black), nighttime (blue), and compound heatwaves (red) during 1999–2022. Dashed lines of different colors represent linearly fitted results with respect to each type. The rectangle in (a-f) denote the domain of southern China (17.5°–26°N, 106.5°–117°E). (For interpretation of the references to colour in this figure legend, the reader is referred to the web version of this article.)

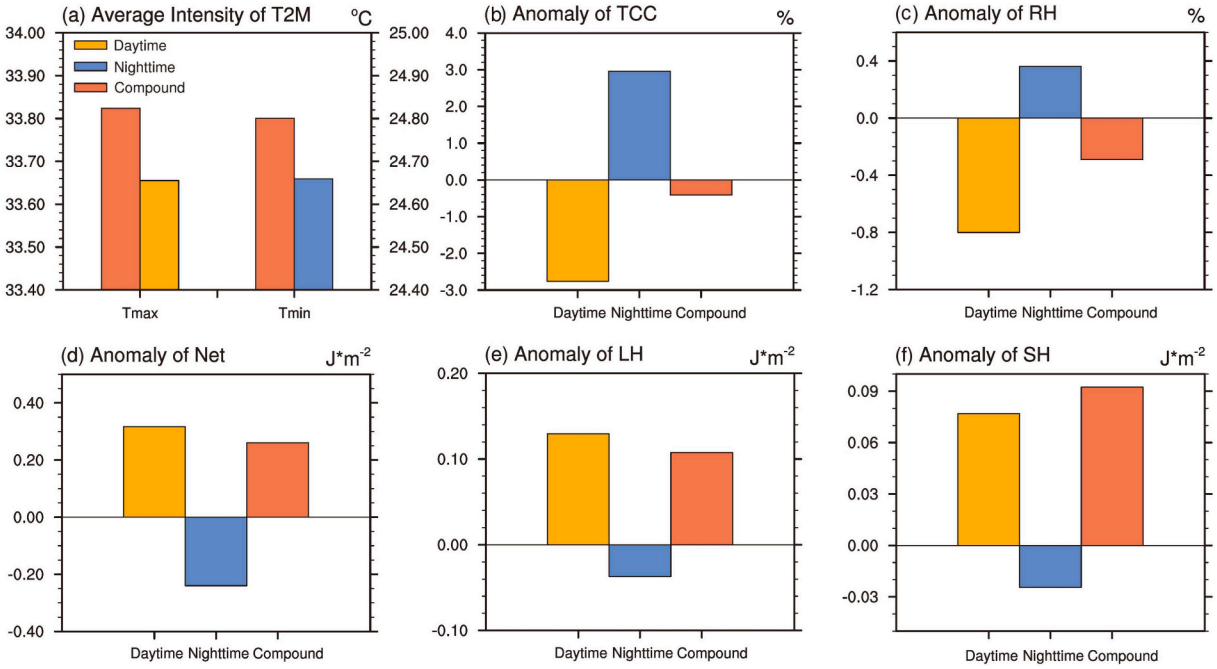


**Fig. 2.** Composite anomalies of reginal-averaged (a) Tmax (°C) and Tmin (°C), (b) total cloud cover (%), (c) relative humidity (%), (d) surface net radiation flux (W $m^{-2}$; positive downwards), (e) surface latent heat flux (W $m^{-2}$; positive upwards), and (f) surface sensible heat flux (W $m^{-2}$; positive upwards) for daytime, nighttime, and compound heatwaves over southern China during MJJAS 1999–2022.

and latent heat fluxes (Fig. 2e–f). Local processes during compound heatwaves over southern China resemble those of daytime heatwaves, yet with markedly weaker negative anomalies in cloud cover and relative humidity (Fig. 2b–f), allowing intense daytime heat persist into the night. In fact, compound heatwaves are substantially more intense than both daytime and nighttime heatwaves and tend to persist for longer (Fig. 2a).

These local anomalies are closely linked to distinct large-scale

atmospheric circulation patterns associated with different heatwave types (Fig. 3). During daytime heatwaves, southern China is situated at the southern edge of an anomalous upper-level anticyclone and the center of an anomalous lower-level anticyclone, which facilitates subsidence and maintains hot and dry conditions as indicated in Fig. 3a, d. The anomalous anticyclonic circulations are more likely induced by Rossby wave trains originating from mid-high latitudes, rather than from tropics (Fig. 3a, Fig. S2a–b). This southeastward-propagating wave train signal from mid-high latitudes is also evident prior to the onset of daytime heatwaves (Fig. S2a–b). After the onset, tropical-origin disturbances appear to gradually replace the anomalous anticyclone over southern China with anomalous cyclonic circulation, which may contribute to the termination of daytime heatwaves (Fig. S2d–e and i–j). During nighttime heatwaves, the associated anticyclonic circulation anomalies are located to the southeast of southern China and are typically driven by a "+ - +" Rossby wave pattern propagating northeastward from tropics (Fig. 3b, Fig. S3c). As a result, the southerly flow on the northwestern flank of the anticyclone brings anomalous moisture transport to the region, thereby facilitating the occurrence and sustenance of nighttime heatwaves (Fig. 3e, Fig. S3h). Both the wave train signal and the circulation field weaken remarkably after the onset (Fig. S3 d–e, i–j). In the case of compound heatwaves, the associated anomalous anticyclone is located spatially between its counterparts linked to daytime and nighttime heatwaves, which consequently induces the anomalous moisture transport in an intermediate state (Fig. 3c, f, Fig. S4c, h). Compared to the other two types of heatwaves, compound heatwaves are accompanied by more pronounced geopotential height anomalies, corresponding to a stronger thermal anomaly. The associated anticyclonic system seems to be modulated by Rossby wave trains originating from both mid-high latitudes and low latitudes (Fig. 3c, f, Fig. S4). These signals dissipate rapidly after the onset (Fig. S4d–e, i–j).

## 4. Role of intra-seasonal oscillations

Previous studies have demonstrated that intra-seasonal oscillations could induce alternative anticyclonic and cyclonic circulations over southern China, and hence affect the occurrence of heatwaves (Chen et al., 2016, 2018). To investigate the contributions of intra-seasonal oscillations (10–60-day) to the occurrence of three types of heatwaves, we begin with analyzing the proportion of Tmax and Tmin anomalies attributable to the intra-seasonal component for daytime, nighttime, and compound heatwaves over southern China. For daytime heatwaves, intra-seasonal components contribute approximately 50% to Tmax but less than 20% to Tmin (Fig. 4a, d). In contrast, during nighttime heatwaves, their contributions to Tmax and Tmin are opposite (Fig. 4b, e). Compared to daytime and nighttime heatwaves, compound heatwaves exhibit higher contributions from intra-seasonal components (around 60%) to both Tmax and Tmin (Fig. 4c, f).

We further perform a composite analysis on the intra-seasonal components (10–60-day, 10–30-day, and 30–60-day oscillations) of geopotential height and atmospheric circulation anomalies associated with the different types of heatwaves. Overall, the 10–60-day intra-seasonal component exhibit patterns largely consistent with the original signatures across all three heatwave types (Fig. 5a–c vs Fig. 3a–c; Figs. S2–S4 a–c vs Fig. S5), highlighting a crucial role of intra-seasonal oscillations in heatwave occurrences. Among the three heatwave types, the impact of intra-seasonal oscillations on compound heatwaves is the most pronounced (Fig. 5). We further decompose the intra-seasonal oscillation signals into high-frequency (10–30-day) and low-frequency (30–60-day) components (Fig. 5d–i). Both the high- and low-frequency components exhibit structures similar to those of the 10–60-day intra-seasonal component. Nevertheless, the high-frequency component constitutes the dominant signal, while the influence of the low-frequency component is comparatively weaker (Fig. 5d–i).

The tropical intra-seasonal oscillations significantly influence heatwaves in southern China (Diao et al., 2018; Hsu et al., 2020), and

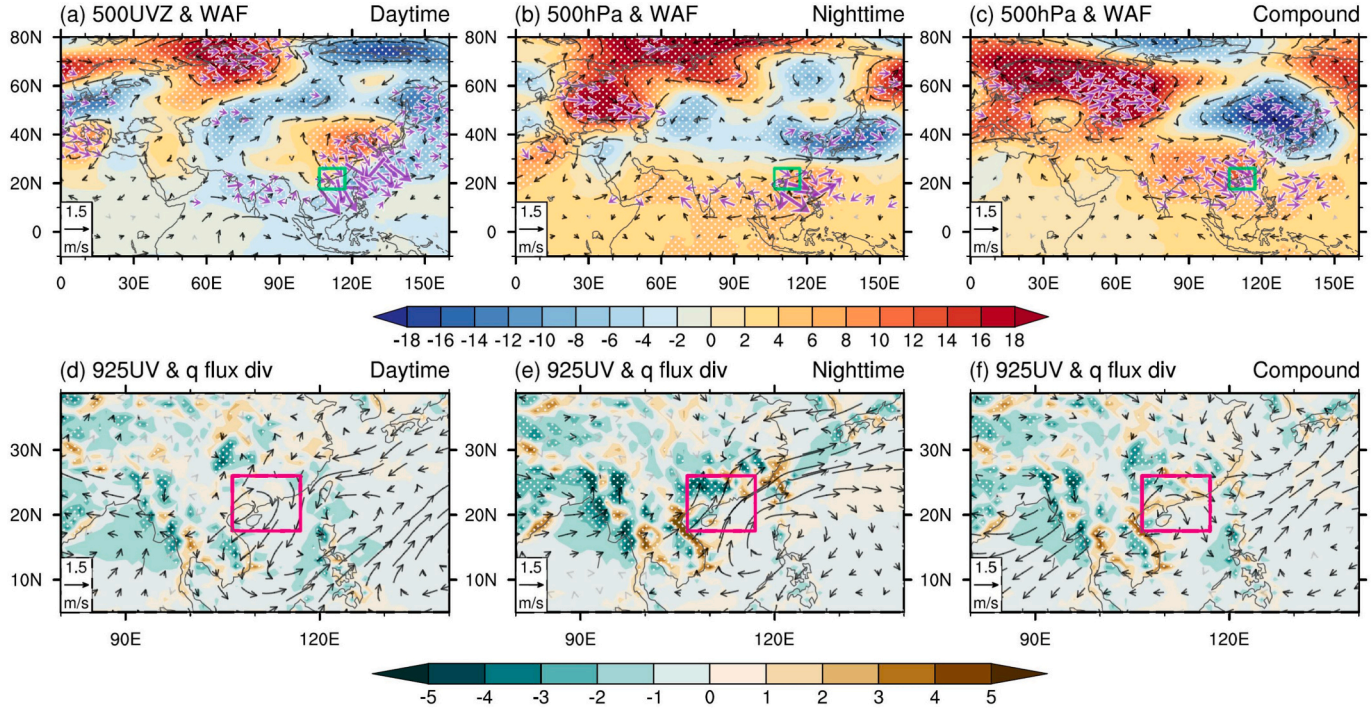


**Fig. 3.** (a–c) Composite anomalies of (a) 500-hPa geopotential height (shading; m), winds (black vectors; m $s^{-1}$), and wave activity flux (purple vectors; $m^2$ $s^{-2}$) for daytime (left), nighttime (middle), and compound heatwaves over southern China (right). (d–f) Same as in (a–c), but for 925-hPa winds (black vectors; m $s^{-1}$) and water vapor flux divergence (shading; kg $m^{-2}$ $s^{-1}$). Stippling areas indicate the values that are statistically significant at the 95% confidence level. The rectangle marks the domain of southern China.

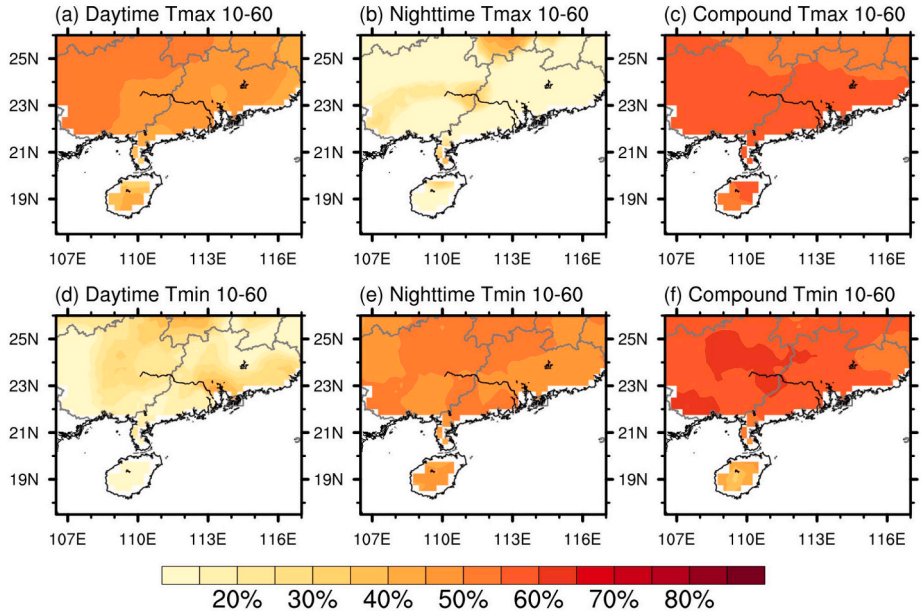


**Fig. 4.** (a–c) Proportion (%) of Tmax anomalies contributed by intra-seasonal components (10–60-day) for daytime (left), nighttime (middle), and compound heatwaves (right) over southern China. (d–f) same as in (a–c), but for the Tmin anomalies.

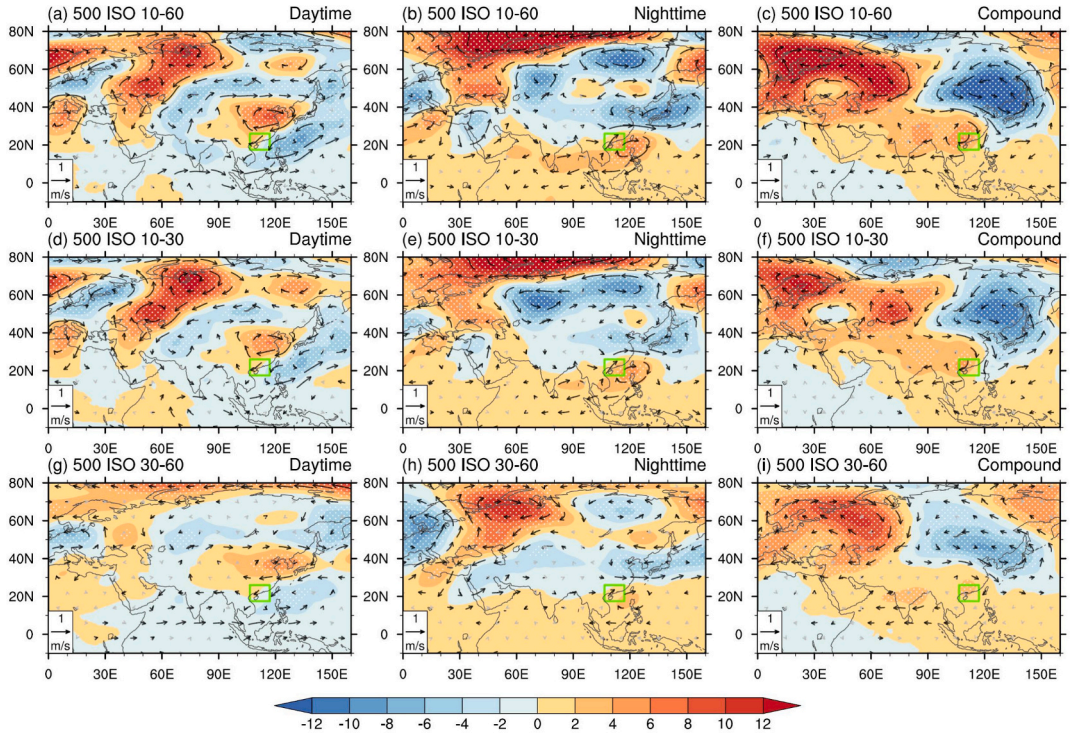


**Fig. 5.** (a–c) Composite anomalies of 500-hPa geopotential height and (shading; gpm) and wind (vectors; m $s^{-1}$) at 10–60-day intra-seasonal timescale for daytime (left), nighttime (middle), and compound heatwaves over southern China (right), respectively. (d–f) and (g–i) are the same as (a–c), but for 10–30-day and 30–60-day intra-seasonal components, respectively. Stippling areas indicate the values that are statistically significant at the 95% confidence level. The rectangle marks the domain of southern China.

structures similar to the BSISOs are also observed in the above analysis. Therefore, based on the BSISO phase indices, we investigate the impacts of different BSISOs on the three types of heatwaves over the region. Fig. 6 displays frequency of daytime, nighttime, and compound heatwaves over southern China in different phases of BSISO1 and BSISO2. Compared to nighttime heatwaves, daytime heatwaves exhibit a weaker phase dependency, with a slightly higher occurrence during BSISO1 phase-4 and BSISO2 phase-2 (Fig. 6a–b and d–e). On the other hand, nighttime heatwaves are more likely to occur in phase-2 of BSISO1 and phases 5–6 of BSISO2 (Fig. 6b, e), during which a high-pressure anomaly is induced to the southeast of southern China (Chen et al., 2018; Lee et al., 2013; Hsu et al., 2020). The likelihood of compound heatwaves is significantly higher during phase-2 of BSISO1, but less phase-dependent for BSISO2 (Fig. 6c, f). The weaker phase-dependent features of

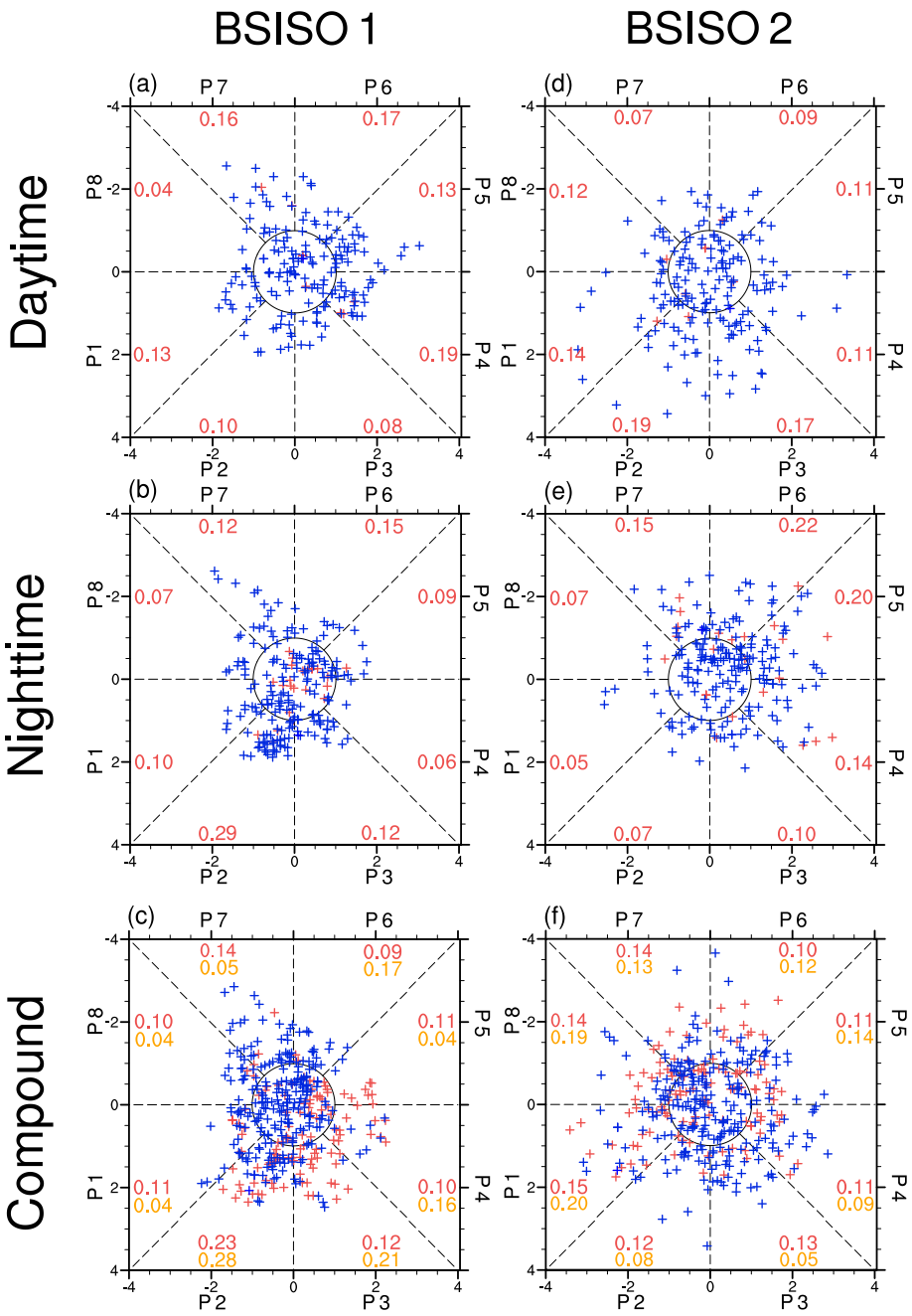


**Fig. 6.** Frequency of southern China (a) daytime, (b) nighttime, and (c) compound heatwaves (right) in different phases of BSISO1. (d–f) are the same as (a–c), but for different phases of BSISO2. Red values indicate the ratio of heatwave frequency in each phase to the total heatwave frequency. Yellow values indicate the ratio of compound heatwave frequency in each phase to the total compound heatwave frequency captured by the NCEP CFSv2 at a 15-day lead. The red and blue makers denote the events successfully captured and missed by the NCEP CFSv2 at a 15-day lead, respectively. (For interpretation of the references to colour in this figure legend, the reader is referred to the web version of this article.)

compound heatwaves might be attributed to the conducive circulation fields associated with multiple BSISO2 phases, and the interference from extra-tropical oscillations.

## 5. Influence of intra-seasonal oscillations on the sub-seasonal prediction of different heatwave types

The extent to which the intra-seasonal oscillations influence the sub-seasonal prediction of daytime, nighttime, and compound heatwaves remains unexplored. In this section, the skills of the NCEP CFSv2 and ECMWF models in predicting the three types of heatwaves over southern China are evaluated, and the role of intra-seasonal oscillations is investigated.

Fig. 7 displays the HSS and EDI of heatwave predictions at different forecast leads, derived from the NCEP CFSv2 and ECMWF. Only when the HSS and EDI values are statistically significant and positive can the model be considered effective in predicting heatwaves. The forecast skills of daytime, nighttime, and compound heatwaves decrease sharply as the lead time increases from 5 to 15 days (Fig. 7). Notably, both the NCEP CFSv2 and ECMWF show higher HSS and EDI values for compound heatwaves compared to daytime and nighttime heatwaves across most lead times (Fig. 7). While compound heatwaves can be effectively predicted approximately 20–35 days in advance, reliable forecasts for daytime and nighttime heatwaves rarely extend beyond a two-week

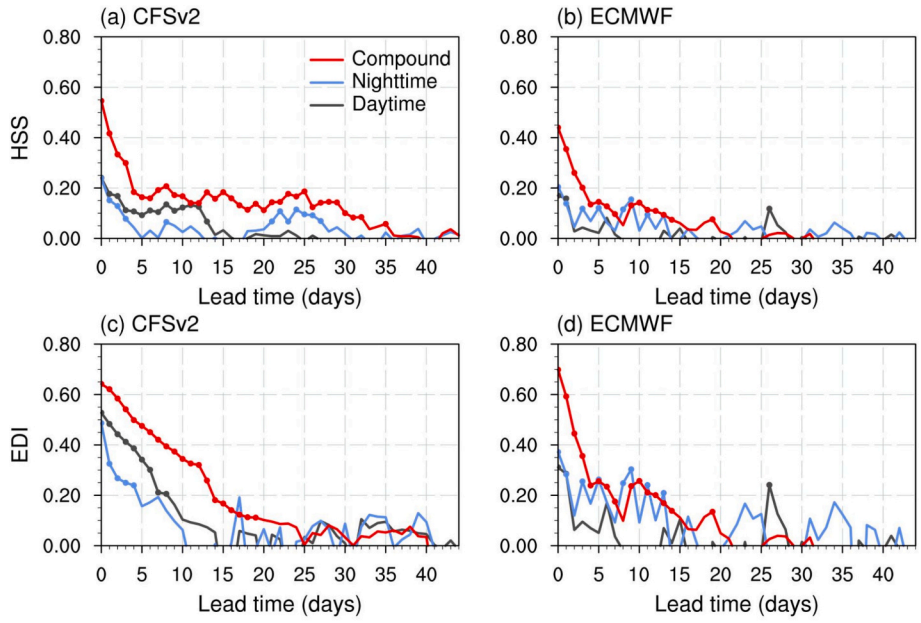


**Fig. 7.** Heidke Skill Score at different forecast leads from 0 to 44 days for daytime (black), nighttime (blue), and compound (red) heatwaves over southern China derived from (a) the CFSv2 and (b) the ECMWF. (c–d) are the same as (a–b), but for the Extreme Dependency Index. Dots indicate the values that are statistically significant at the 95% confidence level based on a bootstrap resampling approach. (For interpretation of the references to colour in this figure legend, the reader is referred to the web version of this article.)

horizon. These findings suggest that the models retain a certain level of skill in forecasting compound heatwaves over southern China at sub-seasonal timescale, suggesting their superior predictability compared to daytime and nighttime heatwaves. The higher prediction skill of compound heatwaves may be partly attributed to their greater intensity (Fig. 2a) and stronger linkage to intra-seasonal oscillations (Fig. 4).

We further assess the impact of intra-seasonal oscillations on the sub-seasonal prediction of heatwaves. Given the lack of sub-seasonal prediction skill for daytime and nighttime heatwaves, the following analysis is focused exclusively on compound heatwaves. Based on the performance of the NCEP CFSv2 at a 15-day lead, we calculate the composite temperature anomalies and the contributions from intra-seasonal oscillations for both successfully forecasted (hit) and missed (not hit) compound heatwaves (Fig. 8). Slightly stronger temperature anomalies are observed over southern China for the "hit" group compared to the "not hit" group (Fig. 8a–b, and e–f). Furthermore, the contribution from intra-seasonal oscillations is more pronounced in these successfully forecasted cases, exceeding 70% in most areas (Fig. 8c–d, and j–h). Similar features can be obtained based on the ECMWF performance (figure not shown). These results suggest the significant influence of intra-seasonal oscillations on the sub-seasonal prediction of compound heatwaves.

A comparative analysis of the relevant circulation fields is conducted for "hit" versus "not hit" events to identify a potential sub-seasonal predictability window for compound heatwaves in southern China. Composite anomalies of 500-hPa geopotential height, winds, and wave activity fluxes on different intra-seasonal timescales for compound heatwaves successfully forecasted (hit) and missed (not hit) by the NCEP CFSv2 at 15-day lead are displayed in Fig. 9. In the "hit" group, a robust and well-organized intra-seasonal Rossby wave train is clearly observed propagating northeastward along East Asia from the low-latitudes (Fig. 9a). In contrast, the "not hit" group is accompanied by more pronounced signals from the mid-high latitudes, whereas a weaker northeastward propagation of Rossby wave train from low-latitudes is

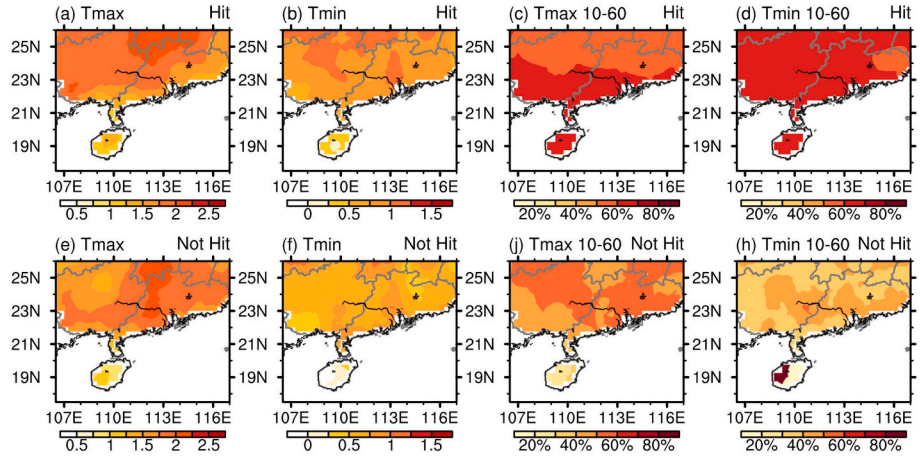


**Fig. 8.** Composite anomalies of (a) Tmax (°C) and (b) Tmin (°C) for compound heatwaves hit by the NCEP CFSv2 at 15-day lead. (c) Proportions of Tmax associated from 10 to 60-day component to total Tmax for compound heatwaves hit by the CFSv2 at a 15-day lead. (d–h) are the same as (a–d), but for compound heatwaves not hit by the CFSv2.

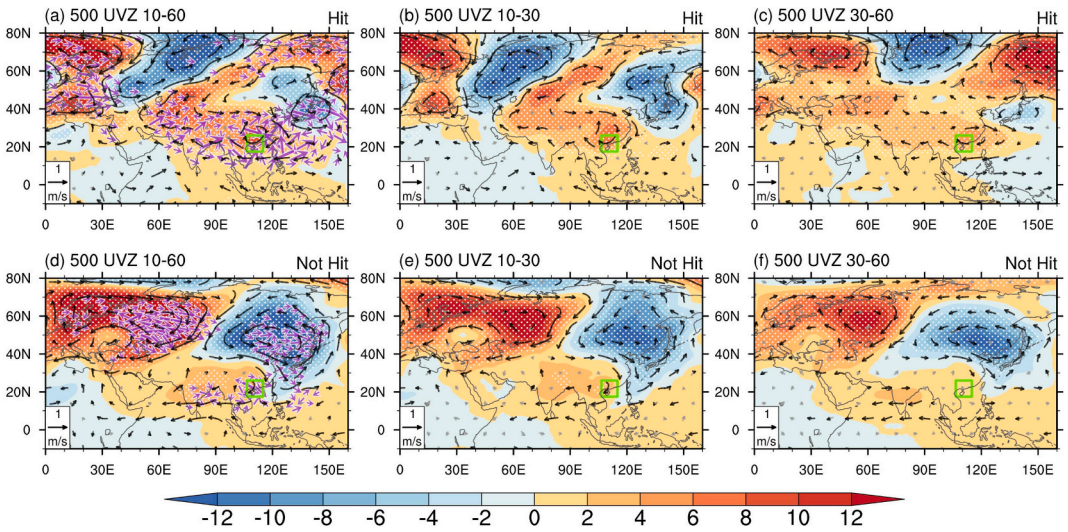


**Fig. 9.** (a–c) Composite anomalies of observed 500-hPa geopotential height (shading; gpm), winds (vectors; m $s^{-1}$), and wave activity flux (purple vectors; $m^2$ $s^{-2}$) at 10–60-day, 10–30-day, 30–60-day intra-seasonal timescales for compound heatwaves hit by the NCEP CFSv2 at a 15-day lead. (d–f) Same as in (a–c), but for the "not hit" group. Stippling areas indicate the values that are statistically significant at the 95% confidence level. The rectangle marks the domain of southern China.

observed (Fig. 9d). The intra-seasonal components of positive geopotential height anomalies dominated over southern China are weaker in the "not hit" group than the "hit" group, contributed by both the weaker high-frequency and low-frequency components (Fig. 9). The composite results based on the performance of the ECMWF model show similar features, including more pronounced northeastward propagation of intra-seasonal Rossby wave train from low-latitudes and a more robust high-pressure system over southern China for the "hit" group compared to the "not hit" group (Fig. 10). The mid-high latitude signals, however, are also more pronounced in the "hit" group than the "not hit" group derived from the ECMWF results (Fig. 10). The above analysis suggests that the enhanced influence of intra-seasonal oscillations, especially those of tropical origin, offers a potential opportunity of sub-seasonal prediction for compound heatwaves in southern China. In fact, the accurately predicted compound heatwaves by the NCEP CFSv2 in 15-day lead tend to be distributed in phases 2–3 of BSISO1 and Phases 8–1 of BSISO2 (Fig. 6). By contrast, daytime and nighttime heatwaves are rarely successfully captured by the model with a 15-day lead, especially daytime heatwaves (Fig. 6). Interestingly, while successfully predicted nighttime heatwaves are concentrated when BSISO1 is insignificant, they are mostly detected in phases 5–7 of BSISO2, signifying the important influence of BSISO2 on the sub-seasonal prediction of nighttime heatwaves in southern China (Fig. 6).

## 6. Conclusion and discussion

As one of the most densely populated and climate-sensitive regions, southern China has been increasingly affected by frequent heatwaves in recent decades, especially compound heatwaves. Understanding the physical mechanisms and sources of predictability for such events, including how they differ from other heatwave types, is essential for improving regional heatwave forecasts. In this study, the distinct influences of tropical and extra-tropical intra-seasonal oscillations on different heatwave types over southern China, along with their implications for sub-seasonal prediction, are comprehensively investigated.

Our findings reveal that daytime heatwaves over southern China are more strongly influenced by extratropical wave trains and typically associated with clear-sky and dry conditions, which promote intense surface heating during daytime (Fig. 11a). Southern China is situated at the southern edge of an anomalous upper-level anticyclone and the

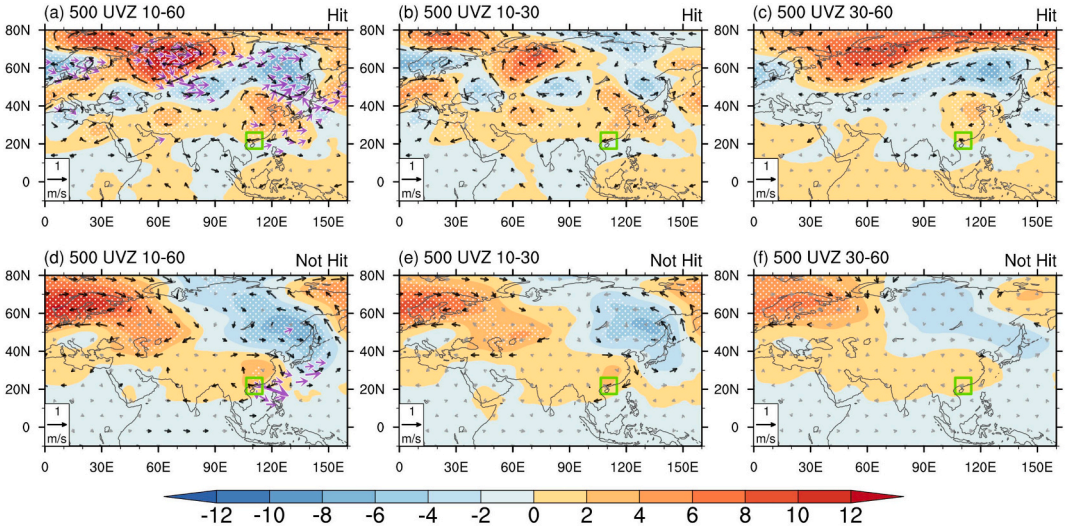


**Fig. 10.** Same as in Fig. 9, but for composite results based on predictions by the ECMWF at a 15-day lead.

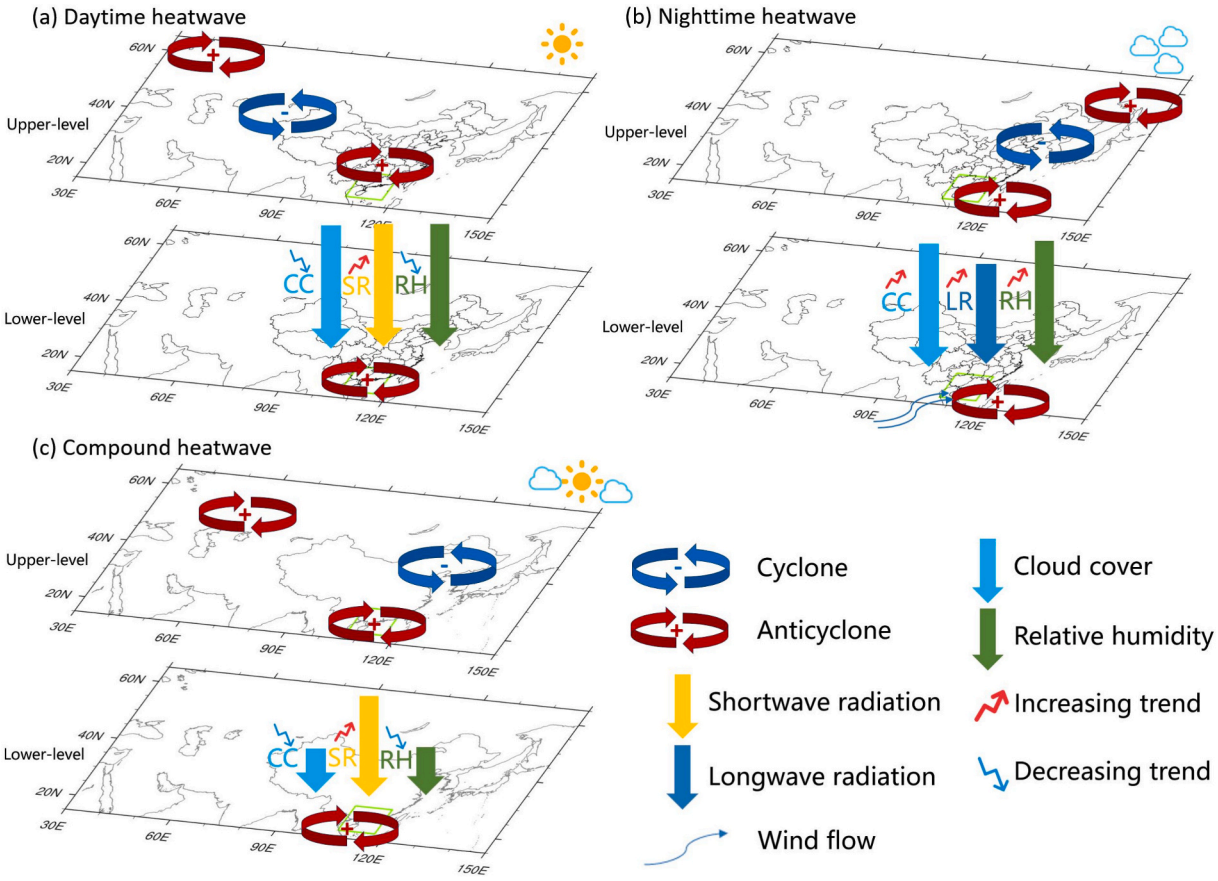


**Fig. 11.** Schematic of physical processes associated with daytime, nighttime, and compound heatwaves over southern China.

center of an anomalous lower-level anticyclone (Fig. 11a). In contrast, nighttime heatwaves are primarily driven by Rossby wave trains propagating northeastward from tropics, which induce anomalous anticyclonic circulation to the southeast of southern China (Fig. 11b). The southerly flow on the northwestern flank of the anticyclone brings anomalous moisture transport to the region, with enhanced cloud cover and humidity, thereby suppressing nocturnal cooling (Fig. 11b). Compound heatwaves are characterized by the most intense surface temperature anomalies and strongest long-term trends among the three heatwave types. Dynamically, compound heatwaves are associated with Rossby wave trains originating from both tropical and extratropical regions (Fig. 11c). These wave trains are largely driven by intra-seasonal oscillations, with the 10–30-day component being predominant. Among the three heatwave types, compound heatwaves exhibit the largest proportion of intra-seasonal variability in both Tmax and Tmin. Nighttime heatwaves exhibit the most pronounced phase-dependent features compared to the other two heatwave types, which are most likely to occur during phase 2 of BSISO1 and phases 5–6 of BSISO2.

Utilizing the NCEP CFSv2 and ECMWF outputs, sub-seasonal prediction skill evaluated via the HSS and EDI shows that compound heatwaves over southern China maintain superior prediction skills compared to daytime and nighttime types. While the effective skill of the other two heatwave types is limited to weather timescales, compound heatwaves retain reliable skills at sub-seasonal range. The higher prediction skill of compound heatwaves may be partly attributed to their greater intensity and stronger linkage to intra-seasonal oscillations. Further composite analysis reveals that successfully forecasted compound heatwaves at a 15-day lead is accompanied by more pronounced northeastward propagation of intra-seasonal Rossby wave train from low-latitudes and a more robust high-pressure system over southern China compared to the events not captured by the models. This finding highlights a potential opportunity of sub-seasonal prediction for compound heatwaves in southern China, which arises from the enhanced influence of intra-seasonal oscillations, particularly those of tropical origin.

While predicting heatwaves beyond two weeks in advance remains a major challenge, the relatively high sub-seasonal prediction skill of recent, markedly intensified compound heatwaves offers a promising new avenue for extended-range early warnings. Despite these findings, several limitations should be acknowledged. Our study is confined to southern China to facilitate a detailed analysis, the broader applicability of our findings remains further research. Furthermore, while our study specifically focuses on the role of intraseasonal oscillations, the evolution of heatwaves involves a combination of dynamical and radiative processes, driven by multi-scale climate systems (Ha et al., 2022; Luo and Lau, 2017; Miralles et al., 2014; Seo et al., 2021; Zscheischler et al., 2020; Zhang et al., 2023). The initialization of land surface conditions, such as soil moisture, and the land–atmosphere feedbacks also pay important roles in affecting heatwaves and their sub-seasonal prediction (Perkins et al., 2015; Lyu et al., 2024; Zheng et al., 2025). For instance, Lyu et al. (2024) demonstrated that the ECMWF model exhibited limited skill in predicting soil moisture reduction and failed to accurately capture land-atmosphere coupling, resulting in a severe underestimation of the 2023 heatwave intensity over Southeast Asia. A composite analysis of soil moisture for “hit” and “not hit” events in the 15-day lead forecast further underscores the critical role of soil moisture in the sub-seasonal prediction of compound extreme heatwaves (Fig. S6). Moreover, the peripheral subsidence and associated moisture transport prior to typhoon landfall may also contribute to the occurrence of heatwaves (Zhao et al., 2021; Zhang et al., 2024). Several heatwaves, particularly daytime and compound ones, were observed before landfall or dissipation, such as the cases in 2008 and 2019 summers (Fig. S1). Whether and

how the interactions between typhoons and intraseasonal oscillations affect the sub-seasonal prediction of different types of heatwaves over southern China remains an open question. As the dominant signal on the interannual timescale, previous studies have indicated that ENSO can also significantly modulate both intraseasonal oscillations and heatwaves (Lin, 2019; Tang et al., 2023). How these various factors and their interplay influence different types of heatwaves and their sub-seasonal prediction remains poorly understood, warranting further investigations.

## CRediT authorship contribution statement

**Kaiqi Wang:** Writing – original draft, Visualization, Software, Formal analysis. **Tuantuan Zhang:** Writing – review & editing, Formal analysis, Conceptualization. **Song Yang:** Writing – review & editing, Formal analysis. **Fei Liu:** Writing – review & editing, Formal analysis. **Weiwei Wang:** Writing – review & editing, Formal analysis. **Wenshi Lin:** Writing – review & editing, Formal analysis. **Lianlian Xu:** Writing – review & editing, Formal analysis, Conceptualization. **Yanheng Luo:** Formal analysis. **Haiyang Xue:** Formal analysis.

## Declaration of competing interest

The authors declare that there is no conflict of interests regarding the publication of this article.

## Acknowledgments

This research was jointly supported by the Guangdong Major Project of Basic and Applied Basic Research (2020B0301030004), the Southern Marine Science and Engineering Guangdong Laboratory (Zhuhai) (SML2024SP012), Guangdong Basic and Applied Basic Research Foundation (2024B1515250004, 2023A1515240064), the National Natural Science Foundation of China (42371028), and the Guangdong Province Key Laboratory for Climate Change and Natural Disaster Studies (2023B1212060019).

## Appendix A. Supplementary data

Supplementary data to this article can be found online at https://doi.org/10.1016/j.atmosres.2026.108915.

## Data availability statement

The CN05.1 datasets are available at https://ccrc.iap.ac.cn/resource, and the ERA5 datasets at https://cds.climate.copernicus.eu. Additional information about the S2S models can be found at https://confluence.ecmwf.int/display/S2S.

## References

Annamalai, H., Slingo, J.M., 2001. Active/break cycles: diagnosis of the intraseasonal variability of the Asian Summer Monsoon. Climate Dynam. 18, 85–102. https://doi.org/10.1007/s003820100161.

Barbero, R., Abatzoglou, J.T., Hegewisch, K.C., 2017. Evaluation of statistical downscaling of North American multimodel ensemble forecasts over the western United States. Weather Forecast. 32, 327–341. https://doi.org/10.1175/WAF-D-16-0117.1.

Bell, J.E., Brown, C.L., Conlon, K., Herring, S., Kunkel, K.E., Lawrimore, J., Luber, G., Schreck, C., Smith, A., Uejio, C., 2018. Changes in extreme events and the potential impacts on human health. J. Air Waste Manage. Assoc. 68, 265–287. https://doi.org/10.1080/10962247.2017.1401017.

Chen, Y., Li, Y., 2017. An inter-comparison of three heat wave types in China during 1961-2010: observed basic features and linear trends. Sci. Rep. 7, 45619. https://doi.org/10.1038/srep45619.

Chen, R., Lu, R., 2014. Dry tropical nights and wet extreme heat in Beijing: atypical configurations between high temperature and humidity. Mon. Weather Rev. 142, 1792–1802. https://doi.org/10.1175/MWR-D-13-00289.1.

Chen, R., Wen, Z., Lu, R., 2016. Evolution of the circulation anomalies and the quasi-biweekly oscillations associated with extreme heat events in southern China. J. Clim. 29, 6909–6921. https://doi.org/10.1175/JCLI-D-16-0160.1.

Chen, R., Wen, Z., Lu, R., 2018. Large-scale circulation anomalies and intraseasonal oscillations associated with long-lived extreme heat events in South China. J. Clim. 31, 213–232. https://doi.org/10.1175/JCLI-D-17-0232.1.

Della-Marta, P.M., Luterbacher, J., Von Weissenfluh, H., Xoplaki, E., Brunet, M., Wanner, H., 2007. Summer heat waves over western Europe 1880–2003, their relationship to large-scale forcings and predictability. Climate Dynam. 29, 251–275. https://doi.org/10.1007/s00382-007-0233-1.

Diao, Y., Li, T., Hsu, P.-C., 2018. Influence of the boreal summer intraseasonal oscillation on extreme temperature events in the northern hemisphere. J. Meteor. Res. 32, 534–547. https://doi.org/10.1007/s13351-018-8031-8.

Ding, T., Qian, W., Yan, Z., 2010. Changes in hot days and heat waves in China during 1961–2007. Int. J. Climatol. 30, 1452–1462. https://doi.org/10.1002/joc.1989.

Dole, R., Hoerling, M., Perlwitz, J., Eischeid, J., Pegion, P., Zhang, T., Quan, X.-W., Xu, T., Murray, D., 2011. Was there a basis for anticipating the 2010 Russian heat wave? Geophys. Res. Lett. 38, L06701. https://doi.org/10.1029/2010GL046582.

Dong, S., Yang, S., Yan, X., Zhang, T., Feng, Y., Hu, P., 2020. The most predictable patterns and prediction skills of subseasonal prediction of rainfall over the Indo-Pacific regions by the NCEP Climate Forecast System. Climate Dynam. 54, 2759–2775. https://doi.org/10.1007/s00382-020-05141-5.

Fang, Y., Wu, P., Mizielinski, M.S., Roberts, M.J., Wu, T., Li, B., Vidale, P.L., Demory, M., Schiemann, R., 2017. High-resolution simulation of the boreal summer intraseasonal oscillation in Met Office Unified Model. Q. J. Roy. Meteorol. Soc. 143, 362–373. https://doi.org/10.1002/qj.2927.

Ferro, C.A.T., Stephenson, D.B., 2011. Extremal dependence indices: improved verification measures for deterministic forecasts of rare binary events. Weather Forecast. 26, 699–713. https://doi.org/10.1175/WAF-D-10-05030.1.

Gao, M., Wang, B., Yang, J., Dong, W., 2018a. Are peak summer sultry heat wave days over the Yangtze-Huaihe river basin predictable? J. Clim. 31, 2185–2196. https://doi.org/10.1175/JCLI-D-17-0342.1.

Gao, M., Yang, J., Wang, B., Zhou, S., Gong, D., Kim, S.-J., 2018b. How are heat waves over Yangtze River valley associated with atmospheric quasi-biweekly oscillation? Climate Dynam. 51, 4421–4437. https://doi.org/10.1007/s00382-017-3526-z.

Gao, T., Luo, M., Lau, N., Chan, T.O., 2020. Spatially distinct effects of two El Niño types on summer heat extremes in China. Geophys. Res. Lett. 47, e2020GL086982. https://doi.org/10.1029/2020GL086982.

Gasparrini, A., Armstrong, B., 2011. The impact of heat waves on mortality. Epidemiology 22, 68–73. https://doi.org/10.1097/EDE.0b013e3181fdcd99.

Ha, K.-J., Seo, Y.-W., Yeo, J.-H., Timmermann, A., Chung, E.-S., Franzke, C.L.E., Chan, J. C.L., Yeh, S.-W., Ting, M., 2022. Dynamics and characteristics of dry and moist heatwaves over East Asia. npj Clim. Atmos. Sci. 5, 49. https://doi.org/10.1038/s41612-022-00272-4.

Heidke, P., 1926. Berechnung des Erfolges und der Güte der Windstärkevorhersagen im Sturmwarnungsdienst. Geogr. Ann. 8 (4), 301–349. https://doi.org/10.1080/20014422.1926.11881138.

Hersbach, H., Bell, B., Berrisford, P., Hirahara, S., Horányi, A., Muñoz-Sabater, J., Nicolas, J., Peubey, C., Radu, R., Schepers, D., Simmons, A., Soci, C., Abdalla, S., Abellan, X., Balsamo, G., Bechtold, P., Biavati, G., Bidlot, J., Bonavita, M., Thépaut, J.-N., 2020. The ERA5 global reanalysis. Q. J. R. Meteorol. Soc. 146, 1999–2049. https://doi.org/10.1002/qj.3803.

Higgins, R.W., Kim, H.K., Unger, D., 2004. Long-lead seasonal temperature and precipitation prediction using tropical Pacific SST consolidation forecasts. J. Clim. 17, 3398–3414. https://doi.org/10.1175/1520-0442(2004)017%3C3398:LSTAPP%3E2.0.CO;2.

Hong, J., Yeh, S., Seo, K., 2018. Diagnosing physical mechanisms leading to pure heat waves versus pure tropical nights over the Korean Peninsula. J. Geophys. Res. 123, 7149–7160. https://doi.org/10.1029/2018jd028360.

Hsu, P.-C., Qian, Y., Liu, Y., Murakami, H., Gao, Y., 2020. Role of abnormally enhanced MJO over the Western Pacific in the formation and subseasonal predictability of the record-breaking northeast Asian heatwave in the summer of 2018. J. Clim. 33, 3333–3349. https://doi.org/10.1175/JCLI-D-19-0337.1.

Huang, Y., Hsu, P.C., Yuan, J., Zhang, W., Lei, L., Xie, J., 2025. Mechanisms of tropical intraseasonal oscillations modulating humid heatwaves in the Asian monsoon region. J. Clim. 38, 3921–3936. https://doi.org/10.1175/JCLI-D-24-0606.1.

Hyvärinen, O., 2014. A probabilistic derivation of Heidke skill score. Weather Forecast. 29, 177–181. https://doi.org/10.1175/WAF-D-13-00103.1.

Jia, X., Yang, S., 2013. Impact of the quasi-biweekly oscillation over the western North Pacific on East Asian subtropical monsoon during early summer. J. Geophys. Res. 118, 4421–4434. https://doi.org/10.1002/jgrd.50422.

Jiang, X., Li, T., Wang, B., 2004. Structures and mechanisms of the northward propagating boreal summer intraseasonal oscillation. J. Clim. 17, 1022–1039. https://doi.org/10.1175/1520-0442(2004)017<1022:SAMOTN>2.0.CO;2.

Kowal, K.M., Slater, L.J., Garcia Lopez, A., Van Loon, A.F., 2023. A comparison of seasonal rainfall forecasts over Central America using dynamic and hybrid approaches from Copernicus Climate Change Service seasonal forecasting system and the North American Multimodel Ensemble. Int. J. Climatol. 43, 2175–2199. https://doi.org/10.1002/joc.7969.

Krishnamurti, T.N., Ardanuy, P., 1980. The 10 to 20-day westward propagating mode and "breaks in the monsoons". Tellus 32, 15–26. https://doi.org/10.1111/j.2153-3490.1980.tb01717.x.

Lau, W.K.M., Kim, K.-M., 2012. The 2010 Pakistan flood and Russian heat wave: teleconnection of hydrometeorological extremes. J. Hydrometeorol. 13, 392–403. https://doi.org/10.1175/JHM-D-11-016.1.

Lee, J.-Y., Wang, B., Wheeler, M.C., Fu, X., Waliser, D.E., Kang, I.-S., 2013. Real-time multivariate indices for the boreal summer intraseasonal oscillation over the Asian summer monsoon region. Climate Dynam. 40, 493–509. https://doi.org/10.1007/s00382-012-1544-4.

Li, Y., Ding, Y., Li, W., 2017. Observed trends in various aspects of compound heat waves across China from 1961 to 2015. J. Meteor. Res. 31, 455–467. https://doi.org/10.1007/s13351-017-6150-2.

Li, Y., Ding, Y., Liu, Y., 2021. Mechanisms for regional compound hot extremes in the mid-lower reaches of the Yangtze River. Int. J. Climatol. 41, 1292–1304. https://doi.org/10.1002/joc.6808.

Li, J., Liao, Z., An, N., Chen, Y., Zhai, P., 2024. Combined influence of 10–30-day tropical and mid–high-latitude intraseasonal oscillations on the rapid increases of humid heatwaves in Southern China. Geophys. Res. Lett. 51 (24), e2024GL112847. https://doi.org/10.1029/2024GL112847.

Li, M., Luo, D., Yao, Y., Zhong, L., 2020. Large-scale atmospheric circulation control of summer extreme hot events over China. Int. J. Climatol. 40 (3), 1456–1476. https://doi.org/10.1002/joc.6279.

Lin, H., 2019. Long-lead ENSO control of the boreal summer intraseasonal oscillation in the East Asian-western North Pacific region. npj. Clim. Atmos. Sci. 2 (1), 31. https://doi.org/10.1038/s41612-019-0088-2.

Loikith, P.C., Broccoli, A.J., 2012. Characteristics of observed atmospheric circulation patterns associated with temperature extremes over north America. J. Clim. 25, 7266–7281. https://doi.org/10.1175/JCLI-D-11-00709.1.

Lu, R.-Y., Chen, R.-D., 2016. A review of recent studies on extreme heat in China. Atmos. Ocean. Sci. Lett. 9, 114–121. https://doi.org/10.1080/16742834.2016.1133071.

Luo, M., Lau, N.-C., 2017. Heat waves in southern China: synoptic behavior, long-term change, and urbanization effects. J. Clim. 30, 703–720. https://doi.org/10.1175/JCLI-D-16-0269.1.

Luo, M., Lau, N.C., Liu, Z., 2022. Different mechanisms for daytime, nighttime, and compound heatwaves in southern China. Weather Clim. Extrem. 36, 100449. https://doi.org/10.1016/j.wace.2022.100449.

Luo, Y., Yang, S., Zhang, T., Yu, Y., Luo, M., Xu, L., 2025. Distinctive local and large-scale processes associated with daytime, nighttime and compound heatwaves in China. Weather. Clim. Extrem. 47, 100749. https://doi.org/10.1016/j.wace.2025.100749.

Lyu, Y., Wang, J., Zhi, X., Wang, X., Zhang, H., Wen, Y., Edward, P., Lee, J., Wan, X., Zhu, S., Dung, D.T., 2024. The characterization, mechanism, predictability, and impacts of the unprecedented 2023 Southeast Asia heatwave. npj. Clim. Atmos. Sci. 7 (1), 246. https://doi.org/10.1038/s41612-024-00797-w.

Mao, J., Chan, J.C.L., 2005. Intraseasonal variability of the south China Sea Summer Monsoon. J. Clim. 18, 2388–2402. https://doi.org/10.1175/JCLI3395.1.

Matsueda, S., Takaya, Y., 2015. The global influence of the Madden-Julian Oscillation on extreme temperature events. J. Clim. 28, 4141–4151. https://doi.org/10.1175/JCLI-D-14-00625.1.

Meehl, G.A., Tebaldi, C., 2004. More intense, more frequent, and longer lasting heat waves in the 21st century. Science 305, 994–997. https://doi.org/10.1126/science.1098704.

Miralles, D.G., Teuling, A.J., Van Heerwaarden, C.C., Vilà-Guerau De Arellano, J., 2014. Mega-heatwave temperatures due to combined soil desiccation and atmospheric heat accumulation. Nat. Geosci. 7, 345–349. https://doi.org/10.1038/ngeo2141.

Oh, H., Ha, K.-J., 2015. Thermodynamic characteristics and responses to ENSO of dominant intraseasonal modes in the East Asian summer monsoon. Climate Dynam. 44, 1751–1766. https://doi.org/10.1007/s00382-014-2268-4.

Pegion, K., Sardeshmukh, P.D., 2011. Prospects for improving subseasonal predictions. Mon. Weather Rev. 139, 3648–3666. https://doi.org/10.1175/MWR-D-11-00004.1.

Perkins, S.E., Alexander, L.V., 2013. On the measurement of heat waves. J. Clim. 26, 4500–4517. https://doi.org/10.1175/jcli-d-12-00383.1.

Perkins, S.E., ArgÜeso, D., White, C.J., 2015. Relationships between climate variability, soil moisture, and Australian heatwaves. J. Geophys. Res. Atmos. 120 (16), 8144–8164. https://doi.org/10.1002/2015JD023592.

Pfahl, S., Schwierz, C., Croci-Maspoli, M., Grams, C.M., Wernli, H., 2015. Importance of latent heat release in ascending air streams for atmospheric blocking. Nat. Geosci. 8, 610–614. https://doi.org/10.1038/ngeo2487.

Qi, X., Yang, J., 2019. Extended-range prediction of a heat wave event over the Yangtze River Valley: role of intraseasonal signals. Atmos. Ocean. Sci. Lett. 12, 451–457. https://doi.org/10.1080/16742834.2019.1669408.

Qian, C., Ye, Y., Jiang, J., Zhong, Y., Zhang, Y., Pinto, I., Huang, C., Li, S., Wei, K., 2024. Rapid attribution of the record-breaking heatwave event in North China in June 2023 and future risks. Environ. Res. Lett. 19, 014–028. https://doi.org/10.1088/1748-9326/ad0dd9.

Robine, J.-M., Cheung, S.L.K., Le Roy, S., Van Oyen, H., Griffiths, C., Michel, J.-P., Herrmann, F.R., 2008. Death toll exceeded 70,000 in Europe during the summer of 2003. C. R. Biol. 331, 171–178. https://doi.org/10.1016/j.crvi.2007.12.001.

Robinson, P.J., 2001. On the definition of a heat wave. Meteor. Clim. 40, 762–775. https://doi.org/10.1175/1520-0450(2001)040<0762:OTDOAH>2.0.CO;2.

Saha, S., Moorthi, S., Wu, X., Wang, J., Nadiga, S., Tripp, P., Behringer, D., Hou, Y., Chuang, H., Iredell, M., Ek, M., Meng, J., Yang, R., Mendez, M.P., van den Dool, H., Zhang, Q., Wang, W., Chen, M., Becker, E., 2014. The NCEP climate forecast system version 2. J. Clim. 27, 2185–2208. https://doi.org/10.1175/JCLI-D-12-00823.1.

Schaefer, J.T., 1990. The critical success index as an indicator of warning skill. Weather Forecast. 5, 570–575. https://doi.org/10.1175/1520-0434(1990)005<0570:TCSIAA>2.0.CO;2.

Schubert, S., Wang, H., Suarez, M., 2011. Warm season subseasonal variability and climate extremes in the northern hemisphere: the role of stationary Rossby waves. J. Clim. 24, 4773–4792. https://doi.org/10.1175/JCLI-D-10-05035.1.

Selesnick, I.W., Burrus, C.S., 2002. Generalized digital Butterworth filter design. IEEE Trans. Signal Process. 46 (6), 1688–1694. https://doi.org/10.1109/78.678493.

Seo, Y.-W., Ha, K.-J., Park, T.-W., 2021. Feedback attribution to dry heatwaves over East Asia. Environ. Res. Lett. 16, 064003. https://doi.org/10.1088/1748-9326/abf18f.

Stephenson, D.B., 2000. Use of the "odds ratio" for diagnosing forecast skill. Weather Forecast. 15, 221–232. https://doi.org/10.1175/1520-0434(2000)015<022 1:UOTORF>2.0.CO;2.

Sun, X., Sun, Q., Zhou, X., Li, X., Yang, M., Yu, A., Geng, F., 2014. Heat wave impact on mortality in Pudong New Area, China in 2013. Sci. Total Environ. 493, 789–794. https://doi.org/10.1016/j.scitotenv.2014.06.042.

Tang, S., Qiao, S., Wang, B., Liu, F., Feng, T., Yang, J., He, M., Chen, D., Cheng, J., Feng, G., Dong, W., 2023. Linkages of unprecedented 2022 Yangtze River Valley heatwaves to Pakistan flood and triple-dip La Niña. npj. Clim. Atmos. Sci. 6 (1), 44. https://doi.org/10.1038/s41612-023-00386-3.

Thomas, N.P., Bosilovich, M.G., Marquardt Collow, A.B., Koster, R.D., Schubert, S.D., Dezfuli, A., Mahanama, S.P., 2020. Mechanisms associated with daytime and nighttime heat waves over the contiguous United States. J. Appl. Meteorol. Clim. 59, 1865–1882. https://doi.org/10.1175/JAMC-D-20-0053.1.

Trenberth, K.E., Fasullo, J.T., 2012. Climate extremes and climate change: the Russian heat wave and other climate extremes of 2010. J. Geophys. Res. 117, 17103. https://doi.org/10.1029/2012JD018020.

Vitart, F., 2014. Evolution of ECMWF sub-seasonal forecast skill scores. Q. J. Roy. Meteorol. Soc. 140, 1889–1899. https://doi.org/10.1002/qj.2256.

Vitart, F., Robertson, A.W., 2018. The sub-seasonal to seasonal prediction project (S2S) and the prediction of extreme events. npj. Clim. Atmos. Sci. 1, 3. https://doi.org/10.1038/s41612-018-0013-0.

Vitart, F., Ardilouze, C., Bonet, A., Brookshaw, A., Chen, M., Codorean, C., Déqué, M., Ferranti, L., Fucile, E., Fuentes, M., Hendon, H., Hodgson, J., Kang, H., Kumar, A., Lin, H., Liu, G., Liu, X., Malguzzi, P., Mallas, I., Manoussakis, M., Mastrangelo, D., MacLachlan, C., McLean, P., Minami, A., Mladek, R., Nakazawa, T., Najm, S., Nie, Y., Rixen, M., Robertson, A.W., Ruti, P., Sun, C., Takaya, Y., Tolstykh, M., Venuti, F., Waliser, D., Woolnough, S., Wu, T., Won, D., Xiao, H., Zaripov, R., Zhang, L., 2017. The subseasonal to seasonal (S2S) prediction project database. Bull. Am. Meteor. Soc. 98, 163–173. https://doi.org/10.1175/BAMS-D-16-0017.1.

Waliser, D.E., Lau, K.M., Stern, W., Jones, C., 2003. Potential predictability of the Madden-Julian Oscillation. Bull. Am. Meteorol. Soc. 84, 33–50. https://doi.org/10.1175/BAMS-84-1-33.

Walker, D.P., Birch, C.E., Marsham, J.H., Scaife, A.A., Graham, R.J., Segele, Z.T., 2019. Skill of dynamical and GHACOF consensus seasonal forecasts of East African rainfall. Climate Dynam. 53, 4911–4935. https://doi.org/10.1007/s00382-019-04835-9.

Wang, P., Tang, J., Sun, X., Wang, S., Wu, J., Dong, X., Fang, J., 2017. Heat waves in China: definitions, leading patterns, and connections to large-scale atmospheric circulation and SSTs. J. Geophys. Res. 122, 10679–10699. https://doi.org/10.1002/2017jd027180.

Wang, S., Ma, D., Sobel, A.H., Tippett, M.K., 2018. Propagation characteristics of BSISO Indices. Geophys. Res. Lett. 45, 9934–9943. https://doi.org/10.1029/2018GL078321.

Wang, J., Feng, J., Yan, Z., Chen, Y., 2020. Future risks of unprecedented compound heat waves over three vast urban agglomerations in China. Earth Future 8, e2020EF001716. https://doi.org/10.1029/2020EF001716.

Wang, K., Zhang, T., Yang, S., Lin, W., Wang, W., Wang, T., Zhang, C., Dong, S., 2025. Roles of the tropical intra-seasonal oscillations in the sub-seasonal prediction of the long-lasting compound heatwave over southern China in 2010. J. Meteor. Res. 31, 30–42. https://doi.org/10.3724/j.1006-8775.2024.033.

Wu, J., Gao, X., 2013. A gridded daily observation dataset over China region and comparison with the other datasets. Chin. J. Geophys. 56, 1102–1111. https://doi.org/10.6038/cjg20130406 cjg20130406.

Wu, S., Luo, M., Zhao, R., Li, J., Sun, P., Liu, Z., Wang, X., Wang, P., Zhang, H., 2023. Local mechanisms for global daytime, nighttime, and compound heatwaves. npj. Clim. Atmos. Sci. 6, 36. https://doi.org/10.1038/s41612-023-00365-8.

Xie, J., Yu, J., Chen, H., Hsu, P.-C., 2020. Sources of subseasonal prediction skill for heatwaves over the Yangtze River Basin revealed from three S2S models. Adv. Atmos. Sci. 37, 1435–1450. https://doi.org/10.1007/s00376-020-0144-1.

Yang, J., Zhu, T., Gao, M., Lin, H., Wang, B., Bao, Q., 2018. Late-July barrier for subseasonal forecast of summer daily maximum temperature over Yangtze River Basin. Geophys. Res. Lett. 45, 12610–12615. https://doi.org/10.1029/2018GL080963.

You, Q., Jiang, Z., Kong, L., Wu, Z., Bao, Y., Kang, S., Pepin, N., 2017. A comparison of heat wave climatologies and trends in China based on multiple definitions. Clim. Dynam. 48, 3975–3989. https://doi.org/10.1007/s00382-016-3315-0.

Zhang, T., Deng, Y., Chen, J., Yang, S., Dai, Y., 2023. An energetics tale of the 2022 mega-heatwave over central-eastern China. npj. Clim. Atmos. Sci. 6 (1), 162. https://doi.org/10.1038/s41612-023-00490-4.

Zhang, M., Yang, Y., Zhan, C., Zong, L., Gul, C., Wang, M., 2024. Tropical cyclone-related heatwave episodes in the Greater Bay Area, China: synoptic patterns and urban-rural disparities. Weather Clim. Extrem. 44, 100656. https://doi.org/10.1016/j.wace.2024.100656.

Zhao, D., Lin, Y., Li, Y., Gao, X., 2021. An extreme heat event induced by Typhoon Lekima (2019) and its contributing factors. J. Geophys. Res. Atmos. 126 (11), e2021JD034760. https://doi.org/10.1029/2021JD034760.

Zheng, B., Gu, D., Lin, A., Peng, D., Li, C., Huang, Y., 2022. Structures and mechanisms of heatwaves related to quasi-biweekly variability over southern China. J. Clim. 35 (24), 7981–7994. https://doi.org/10.1175/JCLI-D-22-0282.1.

Zheng, Y., Zhang, T., Yang, S., Jiang, X., Luo, Y., Yan, H., Deng, K., Zhang, C., 2025. Changes in teleconnection patterns and land–atmosphere coupling amplify the

Spring–Early summer heatwaves over southwestern China. Int. J. Climatol. 45 (4), e8732. https://doi.org/10.1002/joc.8732.
Zhou, B., Wen, Q.H., Xu, Y., Song, L., Zhang, X., 2014. Projected changes in temperature and precipitation extremes in China by the CMIP5 multimodel ensembles. J. Clim. 27, 6591–6611. https://doi.org/10.1175/JCLI-D-13-00761.1.
Zscheischler, J., Martius, O., Westra, S., Bevacqua, E., Raymond, C., Horton, R.M., van den Hurk, B., AghaKouchak, A., Jézéquel, A., Mahecha, M.D., Maraun, D., Ramos, A. M., Ridder, N.N., Thiery, W., Vignotto, E., 2020. A typology of compound weather and climate events. Nat. Rev. Earth. Environ. 1, 333–347. https://doi.org/10.1038/s43017-020-0060-z.